Received 31 August 2018; revised 4 October 2018 and 26 October 2018; accepted 5 November 2018.
Date of publication 9 November 2018; date of current version 6 December 2018.

Digital Object Identifier 10.1109/JXCDC.2018.2880205

Evaluation of Operating Margin and Switching Probability of Voltage-Controlled Magnetic Anisotropy Magnetic Tunnel Junctions

JEEHWAN SONG, IBRAHIM AHMED, ZHENGYANG ZHAO, DELIN ZHANG, SACHIN S. SAPATNEKAR, JIAN-PING WANG, AND CHRIS H. KIM

Department of Electrical and Computer Engineering, University of Minnesota, Minneapolis, MN 55455 USA

CORRESPONDING AUTHOR: C. H. KIM (chriskim@umn.edu)

This work was supported in part by C-SPIN, one of the six SRC STARnet Centers, through MARCO and DARPA and in part by the NSF/SRC E2CDA Program.

ABSTRACT Voltage-controlled magnetic anisotropy (VCMA) has attracted great attention as it allows faster switching and lower energy consumption compared to traditional spin-transfer torque-based magnetization switching. In this paper, we evaluate the operating margin and switching probability of VCMA-based magnetic tunnel junctions using realistic material and device parameters. For this paper, we developed a physics-based SPICE model that incorporates various VCMA parameters such as VCMA coefficient, energy barrier, time constant, and external magnetic field. Switching probability of a VCMA device was obtained by running Monte Carlo simulations including thermal fluctuation effects. A design space exploration was performed using the proposed simulation framework. The highest switching probabilities we were able to achieve were 94.9%, 84.8%, and 53.5%, for VCMA coefficient values of 33, 105, and 290 fJ $\cdot$ V^{-1} $\cdot$ m^{-1}, respectively. Our study shows that for VCMA devices to become viable, their switching probability must be improved significantly either through new physics or material innovation.

INDEX TERMS Magnetic tunnel junction (MTJ), switching probability, VCMA coefficient, voltage-controlled magnetic anisotropy (VCMA).

I. INTRODUCTION

Spin-transfer torque magnetic tunnel junction (STT-MTJ) has been proven as a promising device technology for high-density nonvolatile memory applications. STT phenomenon can flip the magnetization of a ferromagnetic layer using the current flowing through the tunnel barrier itself [1]–[7]. The research community has been focusing on making STT more efficient, such as reducing the write current, improving the switching time, and enhancing the tunnel magnetoresistive ratio (TMR) [7], [8]. Many of these challenges stem from the fact that the current required to switch the magnetization is proportional to the energy barrier separating the two states. For example, a higher energy barrier improves the nonvolatility but requires a higher energy to flip states.

One way to alleviate this problem is to temporarily lower the energy barrier right before applying an STT current using a recently reported voltage-controlled magnetic anisotropy (VCMA) effect [9]–[12]. The amount of current needed to switch the magnetization is lower than conventional STT switching owing to the reduced energy barrier. As shown in Fig. 1, applying a positive voltage to a thick tunnel barrier MTJ device decreases the magnetic anisotropy (MA), resulting in a lower energy barrier. Conversely, the energy barrier is expected to increase for a negative voltage, although this has not been proven experimentally [13]. The tunnel barrier can be made thicker than a normal MTJ since the STT current required for switching is reduced by the VCMA effect. Despite the early experimental results, to our knowledge, there has not been any study on the operating margin and switching probability of VCMA devices.

In this paper, we study these critical aspects of VCMA devices and present design space exploration results. The remainder of this paper is organized as follows.

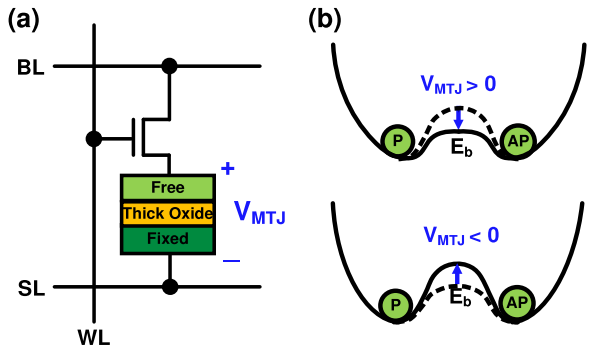

FIGURE 1. (a) VCMA STT-MRAM bit cell. (b) Energy barrier of a VCMA MTJ is modulated by the applied voltage V_E. When the energy barrier is lowered, the magnetization precesses between parallel and antiparallel states.

Section II introduces VCMA effect and its underlying physics. Section III describes the SPICE model developed in this paper. Section IV investigates the effect of material parameters and external field on the switching operation, and then switching probabilities are analyzed in Section V. Conclusions are drawn in Section VI.

II. VCMA BASICS

A. PERPENDICULAR MAGNETIC ANISOTROPY

Depending on the direction of the easy axis, MA can be classified into perpendicular MA (PMA) and in-plane MA (IMA). Compared to an IMA-based device, a PMA-based device has proven to have a lower switching current for the same thermal stability factor (TSF) [14]–[16]. PMA can be further classified based on its origin: interfacial PMA (iPMA) and crystalline PMA (cPMA). iPMA has been observed in CoFeB whose thickness is below the critical thickness t_C where the perpendicular anisotropy occurs, while cPMA has been observed in high crystalline anisotropy materials such as CoPt and FePd [17], [18]. The effective perpendicular anisotropy field ($H_{K\perp\text{eff}}$) can be expressed as

$$H_{K\perp\text{eff}} = H_{K\perp} - H_{dz} = 2K_\perp/M_s - 4\pi N_{dz}M_s \qquad (1)$$

where $H_{K\perp}$ is the perpendicular anisotropy field, $H_d = [H_{dx}, H_{dy}, H_{dz}]$ is the demagnetization field, M_s is the saturation magnetization, and $N_d = [N_{dx}, N_{dy}, N_{dz}]$ is the geometry-dependent demagnetization coefficient. For the interface PMA, $K_\perp$can be expressed as K_i/t_F $(=2\pi M_s^2 t_c/t_F)$ where K_i is the interfacial anisotropy energy density and t_F is the free layer thickness. For the cPMA, $K_\perp = K_u$ where K_u is the crystal anisotropy energy density. Since VCMA effect has traditionally been observed only in iPMA material [19]–[24], we only considered iPMA-based MTJs in this paper.

B. VCMA EFFECT

Recent experiments have shown that by applying a positive voltage to an MTJ, interface PMA can be reduced [25]. The physical origin of this phenomenon is that the charge accumulation or depletion at the metal-barrier interface, which is induced by an electric field, can change the MA through modifying the spin-orbit interaction at the interface [26], [27]. The relationship between the applied voltage and iPMA can be modeled as follows:

$$K_i = K_i|_{V=0} - \xi V / t_{\text{ox}} \qquad (2)$$

where ξ is the VCMA coefficient that represents the sensitivity between MA and the applied electric field, and t_{ox} is the oxide layer thickness. The change in PMA modulates the energy barrier (E_b) of the free layer [28]. Applying a positive voltage to the oxide layer lowers the energy barrier, thus it enables the free layer's magnetization to precess between the two stable states. Compared to STT-induced switching, VCMA switching can be fast due to the lowered energy barrier and consumes less switching energy due to the thicker tunnel barrier layer.

TSF of an MTJ is a critical device parameter that determines the data retention capability of a ferromagnetic layer. It is defined as the free layer's energy barrier normalized to the k_BT energy [29]. VCMA induces change in K_i, which in turn changes the TSF as follows:

$$\text{TSF} = \frac{E_b}{k_BT} = \frac{(K_i - 2\pi M_s^2 t_F)A}{k_BT} \qquad (3)$$

where E_b is the voltage-dependent energy barrier between two stable states, A is the cross-sectional area of the free layer, k_B is Boltzmann's constant, and T is the absolute temperature.

C. THERMAL FLUCTUATION

Intrinsic randomness in the magnetization's behavior referred to as thermal fluctuation may affect the switching characteristics. For example, it can thermally activate the magnetization's initial angle at the beginning of the writing operation, which can either induce "unwanted" switching or impede "wanted" switching [30]. To emulate the effect of thermal fluctuation in the most realistic way, random thermal field was added not only to the initial angle but also to the effective anisotropy field at each time step of the simulation. Since thermal field is a stochastic process, it can be modeled as a zero-mean Gaussian random distribution with a standard deviation ($\sigma_{H_{\text{th}}}$) as follows [31]:

$$\sigma_{H_{\text{th}}} = \sqrt{2k_B\alpha T/(\mu_0\gamma V_F M_s \delta t)} \qquad (4)$$

where α is the Gilbert damping constant, μ_0 is the permeability in vacuum, γ is the gyromagnetic ratio, V_F is the volume of the free layer, and δt is the time step. A $\sigma_{H_{\text{th}}}$ value of 4.5 mT was used for all the Monte Carlo simulations in this paper.

III. VCMA-MTJ SPICE MODEL SETUP

This section describes the VCMA-MTJ device model for simulating two switching schemes: VCMA only switching scheme and VCMA-assisted STT switching scheme.

A. MAGNETIZATION DYNAMICS

The proposed SPICE model is based on the Landau–Lifshitz–Gilbert (LLG) equation which comprises precession, damping, and STT terms as follows:

$$\frac{1+\alpha^2}{\gamma}\cdot\frac{d\vec{M}}{dt} = -\vec{M}\times\vec{H}_{\text{eff}}(V) - \alpha\cdot\vec{M}\times(\vec{M}\times\vec{H}_{\text{eff}}(V)) + \frac{\hbar PJ}{2etM_s}\cdot\vec{M}\times(\vec{M}\times\vec{M}_P) \quad (5)$$

where $\vec{M}$ is the magnetization vector of the free layer, $\vec{H}_{\text{eff}}(V)$ is the voltage-dependent effective magnetic field, $\hbar$ is the reduced Planck's constant, P is the spin-polarization factor, J is the switching current density, e is the electron charge, and $\vec{M}_P$ is the magnetization vector of fixed layer.

More specifically, $\vec{H}_{\text{eff}}(V)$ includes different field components affecting the free layer [32]

$$\vec{H}_{\text{eff}}(V) = \vec{H}_{\text{ext}} + \vec{H}_d + \vec{H}_{\text{th}} + \vec{H}_{K\perp\text{eff}}(V) \quad (6)$$

$$\vec{H}_{K\perp\text{eff}}(V) = \left(0\vec{x}, 0\vec{y}, \left(\frac{2K_i(V)}{\mu_0 M_s t_F}\right)m_z\vec{z}\right) \quad (7)$$

where $\vec{H}_{\text{ext}}$ is the external magnetic field, $\vec{H}_d$ is the demagnetization field, $\vec{H}_{\text{th}}$ is the thermal field, $\vec{H}_{K\perp\text{eff}}(V)$ is the voltage-dependent effective perpendicular anisotropy field, μ_0 is the permeability, $m = [m_x, m_y, m_z]$ is the magnetization moment, and $[\vec{x}, \vec{y}, \vec{z}]$ is the unit vector.

The VCMA effect can be incorporated into the LLG equation in (5) by combining (6) and (7). In addition, VCMA affects the TSF which in turn affects $\vec{M}$ in (5). This is because the magnetization's initial angle is a variable. It can be modeled using the Fokker–Plank distribution as follows [33]:

$$\text{PDF}(\theta)|_{t=0} = \frac{\exp(-\text{TSF}\cdot\sin^2\theta)}{\int_0^{\pi}\sin\theta\exp(-\text{TSF}\cdot\sin^2\theta)d\theta} \quad (8)$$

where $\text{PDF}(\theta)|_{t=0}$ is the initial angle's probability distribution function, TSF is the thermal stability factor, and θ is the magnetization's angle (Fig. 2).

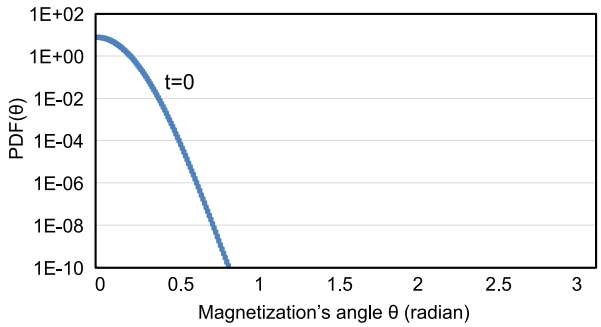

FIGURE 2. Initial angle distribution $\text{PDF}(\theta)|_{t=0}$ for TSF = 45.7.

Since we use the LLG equation and add stochasticity in the initial angle and the run-time random thermal field, our simulation method is equivalent to the stochastic LLG equation in [43].

TMR is expressed as $(R_{\text{AP}} - R_{\text{P}})/R_{\text{P}}$ where R_{AP} and R_{P} are the antiparallel and parallel resistances of the MTJ, respectively. The voltage and temperature dependence of TMR is captured using the modified Julliere's formula as follows [44]

$$\text{TMR}(T, V) = \frac{2P_0^2(1-\alpha_{\text{sp}}T^{3/2})^2}{1-P_0^2(1-\alpha_{\text{sp}}T^{3/2})^2}\cdot\frac{1}{1+(V/V_0)^2} \quad (9)$$

where P_0 is the polarization factor, $\alpha_{\text{sp}}(= 2e^{-5})$ is the material-dependent empirical constant, and V_0 is the bias voltage where TMR is halved.

The VCMA-MTJ's physical behavior can be reproduced by simulating the SPICE model shown in Fig. 3 consisting of four subcircuits: anisotropy, LLG, TMR, and temperature. Further details of the baseline LLG SPICE model can be found in [34] and [35].

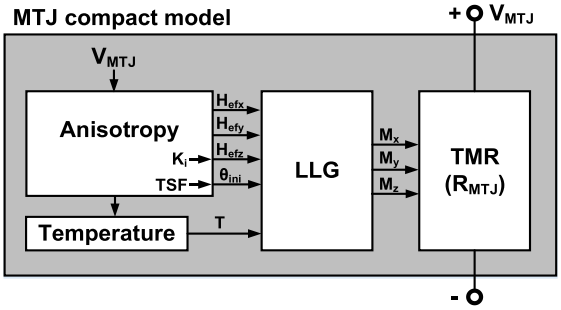

FIGURE 3. Proposed VCMA-based MTJ SPICE compact model.

B. MODEL PARAMETERS

The simulation parameters of the VCMA-MTJ device used in this paper are listed in Table 1. For a more accurate physic-based model, device parameters are taken from state-of-the-art experimental data [19]–[23]. Three different VCMA coefficients ranging from 33 to 290 $\text{fJ}\cdot\text{V}^{-1}\cdot\text{m}^{-1}$ are considered in order to analyze its effect on the switching time and switching probability. We assume a TSF value of 45.7 [5]. To facilitate the switching, a 20-mT external magnetic field was applied along the hard axis (i.e., x-axis) [23], [36], [37].

C. VCMA ONLY SWITCHING

When the energy barrier is lowered by the V_E voltage and external magnetic field is applied at the same time, the VCMA-MTJ's magnetization starts to oscillate around the hard axis due to magnetization dynamics by LLG equation. By terminating the V_E pulse at the appropriate moment, the magnetization can be toggled as illustrated in Fig. 4(a). One limitation of this approach is that the switching direction is nondeterministic, i.e., we can only toggle the magnetization from its initial state. This issue can be circumvented by first reading the state of the MTJ and subsequently applying the write pulse as needed [Fig. 4(b)]. However, this requires an additional read cycle before each write cycle.

TABLE 1. Material parameters used for simulation.

Symbol	Device Parameters	Values
L_X	Free Layer Width [nm]	70 [19]
L_Y	Free Layer Length [nm]	70 [19]
t_F	Free Layer Thickness [nm]	1.49
t_{OX}	Oxide Thickness [nm]	1.4 [19]
t_C	Critical Thickness [nm]	1.5 [21]
RA_P	Resistance-area Product [Ω-μm^2]	130 [19]
TMR_0	Tunnel Magnetoresistance @ 0V [%]	150 [19]
M_{S0}	Saturation Magnetization @ 0K [KA/cm]	950 [20]
P_0	Polarization Factor @ 0K	0.54 [20]
α	Damping Factor	0.025 [21]
ξ	VCMA Coefficient [fJ·V^{-1}·m^{-1}]	33 [19], 105 [22], 290 [23]
TSF	Thermal Stability Factor	45.7
H_{EXT}	External Magnetic Field [mT]	20 (hard-axis)
T	Temperature [K]	358

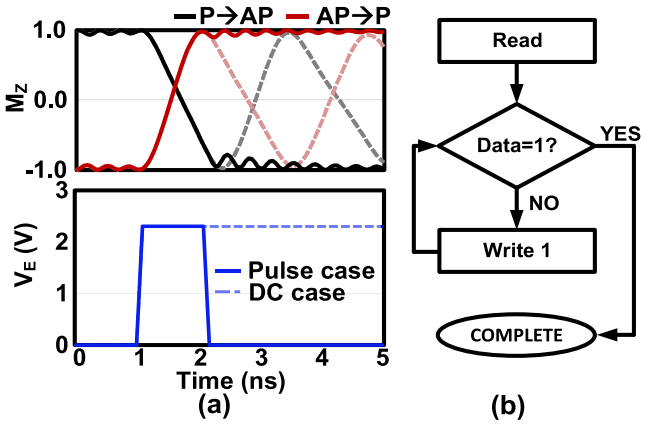

FIGURE 4. VCMA only switching scheme. (a) Write voltage (V_{MTJ}) pulse and magnetization switching simulation results for VCMA device. (b) Flowchart for writing "1" into a VCMA MTJ. Due to the inherent nondeterministic switching of VCMA, a read operation is required before each write operation.

D. VCMA-ASSISTED STT SWITCHING

The VCMA-assisted STT switching scheme proposed in [36] can enable deterministic switching without incurring an extra read operation. Fig. 5 shows the voltage pulse sequence where the initial V_E pulse reduces induces VCMA while the subsequent V_{STT} pulse, perfectly timed at the moment when the magnetization is near the hard axis, tilts the magnetization to either parallel or antiparallel state depending on the voltage polarity. In this paper, we analyzed the switching characteristics of the VCMA-assisted STT switching scheme as it has the advantage of a deterministic switching state. To maximize the switching probability, we optimized the write voltage pulse (i.e., V_E, PW_E, V_{STT}, and PW_{STT} denoted in Fig. 5(a) for each VCMA coefficient value. Fig. 5(b) shows the optimal parameter values found through the optimization method described in Section V.

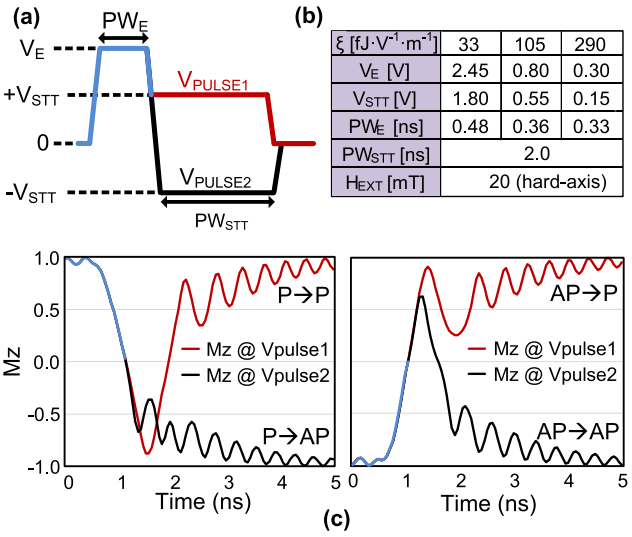

FIGURE 5. VCMA-assisted STT switching scheme. (a) V_{MTJ} waveform where an initial high voltage is followed by a positive or negative STT pulse. (b) Simulation parameters. (c) Magnetization dynamics for P → P, P → AP, AP → P, and AP → AP switching.

IV. MATERIAL PARAMETERS AND EXTERNAL FIELD

In this section, we present simulation results showing the impact of VCMA coefficient, response time of energy barrier, and external magnetic field on VCMA-assisted STT switching.

A. VCMA COEFFICIENT

VCMA coefficient (ξ) is a critical parameter, which determines the sensitivity of the energy barrier to the applied electric field. It can be expressed as follows [38]:

$$\xi[\mathrm{fJ/Vm}] = \frac{\Delta \text{ Interfacial Anisotropy } [\mu \mathrm{J/m^2}]}{\Delta \text{ Electric Field } [\mathrm{V/nm}]}. \quad (10)$$

As shown in Fig. 6, when ξ is increased from 33 to 105 fJ · V^{-1} · m^{-1}, the switching time decreases by 7%. The switching time decreases further by 10% when ξ is increased from 105 to 290 fJ · V^{-1} · m^{-1}. As expected, a higher VCMA coefficient provides faster switching and lower switching energy consumption. The switching energy decreases by 13× when ξ increases from 33 to 105 fJ · V^{-1} · m^{-1}, and by 12× when ξ increases from 105 to 290 fJ · V^{-1} · m^{-1}. Compared to conventional STT-based switching, the switching time decreases by 17%, 23%, and 30%, respectively, for ξ = 33, 105, and 290 fJ · V^{-1} · m^{-1}. The switching energy is reduced by 3×, 40×, and 494×, respectively. In this comparison, we use an MTJ model with a tunneling barrier thickness of 1.0 nm for conventional STT based switching [35]. In addition, compared to SHE-based switching in [31], VCMA-MTJ's switching time is decreased by 17%, 22%, and 30%, respectively, for ξ = 33, 105, and 290 fJ · V^{-1} · m^{-1}, and switching energy is reduced by 8×, 98× for ξ = 105 and 290 fJ · V^{-1} · m^{-1}.

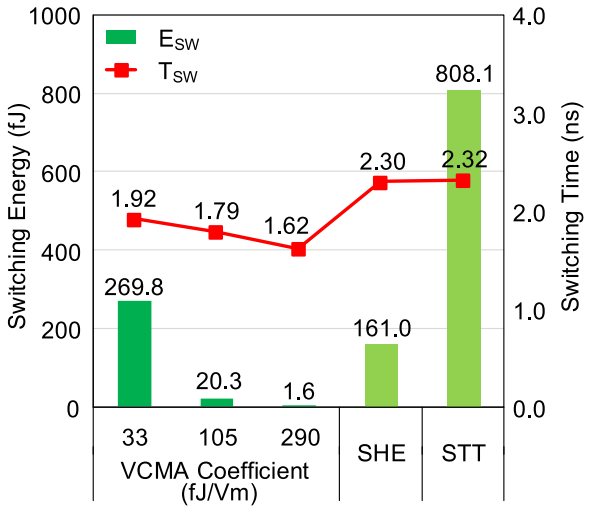

FIGURE 6. Switching energy and switching time for VCMA, SHE, and STT.

Recently, magnetic materials with higher VCMA coefficients have been reported [22], [23], [24], [39]. However, as the VCMA coefficient increases, the free layer's magnetization precesses more rapidly, which makes the switching more unstable and, hence, resulting in a narrower operating window. Consequently, it becomes much more difficult to capture the precise moment when the magnetization swings toward the other side of the hard axis. This can be seen in Fig. 7 where the pulsewidth window for correct switching reduces from 90 to 10 ps as the VCMA coefficient increases from 33 to 290 fJ $\cdot$ V^{-1} $\cdot$ m^{-1}. This trend suggests that extremely precise control of the voltage pulsewidth (e.g., few picoseconds) is required for high VCMA coefficient materials to work reliably.

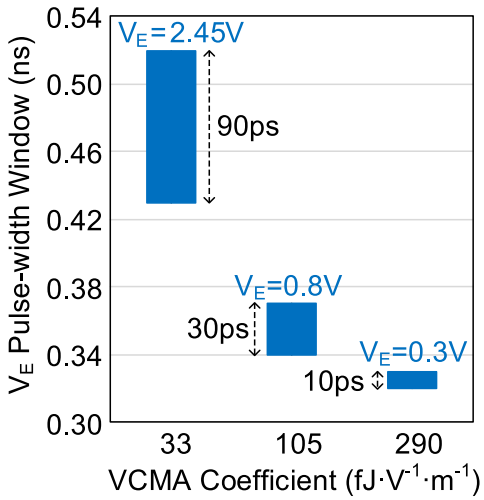

FIGURE 7. Pulsewidth window for different VCMA coefficients.

B. RESPONSE TIME OF ENERGY BARRIER

We also studied the impact of response time (or time constant) between the write voltage and the free layer's energy barrier,

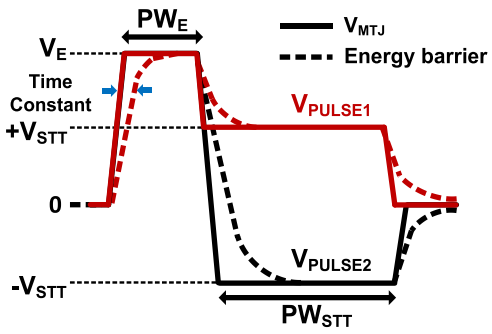

FIGURE 8. Concept of time constant between applied voltage and energy barrier.

on the switching characteristics. Fig. 8 illustrates the concept of time constant, which is the time delay between the solid line (voltage) and dashed line (energy). Since no experimental data on the energy barrier time constant exists, we simply varied the time constant and simulated the switching behavior. The time constant was implemented using a simple first-order *RC* delay circuit in the SPICE model. To implement the time constant effect in our simulation, the MTJ voltage is connected to a first-order *RC* circuit before being applied to the interfacial anisotropy field in the LLG subcircuit.

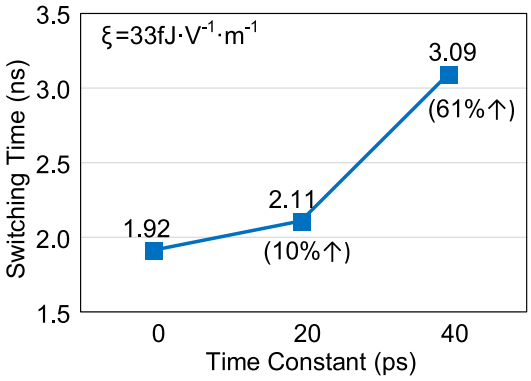

FIGURE 9. Effect of energy barrier time constant on switching time.

As shown in Fig. 9, the switching time increased by 10% and 61%, respectively, for time constant values of 20 and 40 ps. The longer switching time can be attributed to the energy barrier not being fully removed when the V_{STT} pulse arrives. As a result, it takes longer for the magnetization to overcome the residual energy barrier, making VCMA based switching less robust.

C. EXTERNAL MAGNETIC FIELD

In order for the magnetization of a VCMA device to oscillate around the hard axis, an external magnetic field (H_{EXT}) must be applied toward this axis [25], [38]. To this end, we study the effect of external magnetic field by applying different H_{EXT} values and simulating the magnetization switching. As shown in Fig. 10, the switching time reduces from

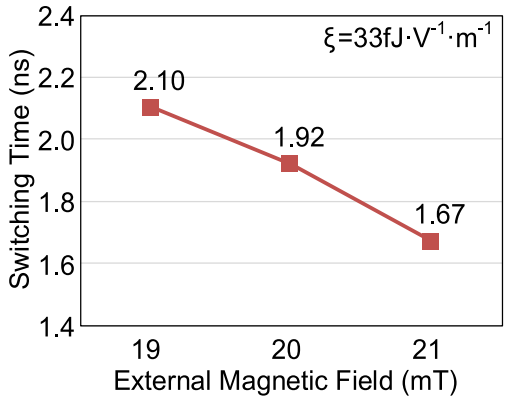

FIGURE 10. **Effect of external magnetic field on switching time.**

2.10 to 1.67 ns as the external magnetic field is increased from 19 to 21 mT. These results indicate that a larger external magnetic field helps tilt the free layer's magnetization toward the hard axis more quickly, which enables faster switching operation.

Applying a magnetic field using off-chip equipment is not feasible for integrated systems. Recent work has shown the feasibility of generating a local magnetic field using a composite device [40]. Here, a composite device was fabricated with an in-plane magnetic layer placed on top of a perpendicular magnetic layer. This paper shows switching of perpendicular Ta/CoFeB/MgO nanopillars in the absence of an external magnetic field. Our model assumes such a composite device where a local magnetic field is generated within each memory cell.

V. SWITCHING PROBABILITY RESULTS

A. MONTE CARLO SIMULATION SETUP

Previous studies on VCMA-assisted STT switching have only reported results for parallel to antiparallel (P-to-AP) and antiparallel to parallel (AP-to-P) switching directions [19], [25], [36], [41]. In this paper, we show switching probability results for all four switching directions, i.e., P-to-AP, P-to-P, AP-to-P, and AP-to-AP. To obtain realistic results, we ran Monte Carlo simulations using 10 000 different initial magnetization angles that were sampled from a probability density function [42]. A thermal fluctuation field of $\sigma_{H_{\text{th}}} = 4.5$ mT was used as per (4).

B. DESIGN SPACE EXPLORATION

The initial simulation parameters were aimed at achieving the lowest possible energy dissipation. First, we selected the minimum V_E that allows the free layer's magnetization to oscillate around the hard axis for both initial states. Then, the V_E pulsewidth was optimized to capture the precise moment when the magnetization is set toward the hard axis. For simplicity, the V_{STT} voltage was fixed to half the V_E voltage, and the V_{STT} pulsewidth was fixed at 2.0 ns. The deterministic switching probabilities using the above-mentioned parameter set were in the 46%–85% range depending on the switching direction. Since these values are far too low for practical memory applications, we adjusted key design parameters such as V_E, PW_E, and V_{STT} in an attempt to improve the switching probability. Our strategy for optimizing the switching probability is summarized next.

1) V_{STT} AMPLITUDE

Increasing the V_{STT} voltage can induce a larger STT current, and thereby induce a stronger STT effect. This forces the magnetization to switch to the desired state, which consequently improves the switching probability. As shown in Fig. 11, the STT current increases by 53% when V_{STT} is increased from 1.2 to 1.8 V, resulting in an improvement of switching probability from 50.1% to 94.9%. However, the switching probability could not be improved further because, at very high V_{STT} voltages, the magnetization has a higher chance of precessing between the two states causing unstable behavior. Therefore, increasing the V_{STT} voltage alone cannot guarantee 100% switching probability. This can be seen in Fig. 11 where the switching probability drops beyond 1.8 V. Note that the optimal V_{STT} voltage was found for each individual V_E voltage. It is also worth mentioning that the spin dynamics of VCMA-assisted switching is fundamentally different from that of STT only switching. For STT only switching, the magnetization is initially aligned with the easy axis, and hence, STT current is responsible for the entire switching operation. For VCMA-assisted switching, however, STT effect is exerted when the magnetization is near the hard axis, allowing a very small STT current to induce switching.

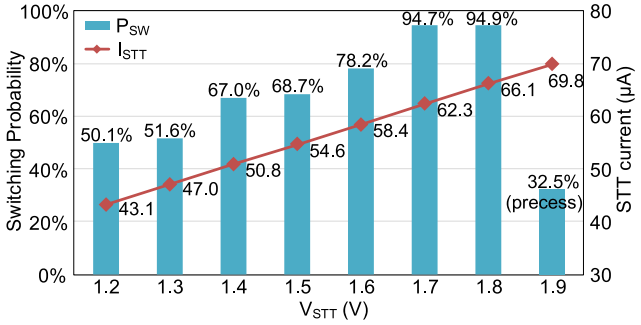

FIGURE 11. **Switching probability versus V_{STT} for $V_E = 2.45$ V.**

2) V_E AMPLITUDE

For our initial simulations, we chose the minimum V_E (i.e., 2.3 V) required for switching because we wanted to minimize the energy consumption. However, during our rigorous simulations, we found that increasing V_E can actually reduce the energy owing to the shorter switching time. At the same time, the switching probability can be enhanced by using a higher V_E voltage. To obtain the maximum switching probability, we optimized the V_E pulsewidth and V_{STT} amplitude for each V_E voltage. We considered a V_E range

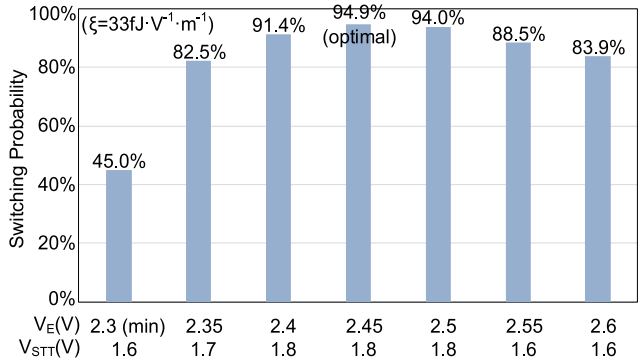

FIGURE 12. Switching probability for different V_E voltages. V_E pulsewidth and V_{STT} voltage were optimized for each V_E voltage.

of 2.3–2.6 V, and first optimized the V_E pulsewidth. Next, as discussed earlier, the V_{STT} voltage offering the highest switching probability was found for each V_E. Fig. 12 compares the switching probability versus V_E obtained from the proposed optimization approach. The switching probability peaks at 94.9% under the condition of $V_E = 2.45$ V and $V_{STT} = 1.8$ V. If V_E is higher than the optimal value, the V_E pulsewidth becomes narrower due to faster precessional motion, resulting in a lower switching probability.

C. EFFECT OF VCMA COEFFICIENT ON SWITCHING PROBABILITY

Finally, the impact of VCMA coefficient on the switching probability was analyzed using Monte Carlo simulations. In this paper, we considered all four switching directions for three different VCMA coefficient cases, i.e., 33, 105, and 290 fJ $\cdot$ V^{-1} $\cdot$ m^{-1}. The V_E and V_{STT} parameters were optimized for the highest switching probability. As shown in Fig. 13, the switching probability depends on the specific switching direction. Results show that even after extensive parameter sweeping, switching probabilities for $\xi = 33$, 105, and 290 fJ $\cdot$ V^{-1} $\cdot$ m^{-1} could not reach the desired value. Moreover, the switching probability generally degrades with

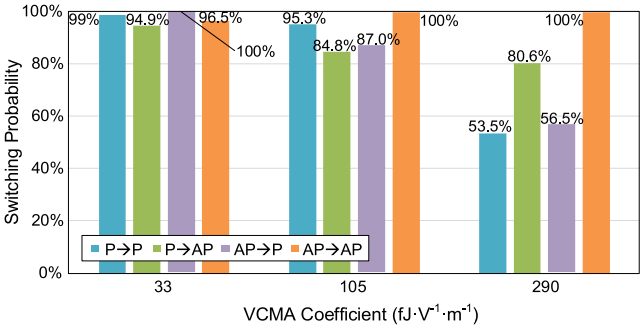

FIGURE 13. Highest switching probability after optimizing V_E, V_{STT}, and pulsewidth for different VCMA coefficients. Switching probabilities for all four directions are shown. Due to the unstable nature of VCMA, it is difficult to achieve switching probabilities required for practical memory applications.

a higher VCMA coefficient because of the narrower operating window (see Fig. 7) which causes more errors to occur in the presence of thermal fluctuation. It is worth noting that the switching probabilities vary significantly based on the switching direction. For the highest VCMA coefficient of 290 fJ $\cdot$ V^{-1} $\cdot$ m^{-1}, the AP $\rightarrow$ AP switching was 100% correct while the P $\rightarrow$ P switching was only 53.5% correct. Despite our best efforts, we were unable to close the gap between different switching probabilities. Our investigation shows that poor switching probability is a major concern for high VCMA coefficient material.

VI. CONCLUSION

In this paper, we evaluated the switching probability of VCMA devices for a wide range of material parameters and external fields, using a SPICE-compatible LLG model. Monte Carlo simulations incorporating thermal fluctuation showed a nine times narrower operating voltage window when the VCMA coefficient increases from 33 to 290 fJ $\cdot$ V^{-1} $\cdot$ m^{-1}. This is due to the unstable switching behavior when the energy barrier becomes more sensitive to the applied voltage. We also varied the time constant between the applied voltage and the energy barrier, as well as the external magnetic field, to understand the impact of switching time. We found that the switching time increases with a longer time constant and with a lower external magnetic field. The maximum switching probabilities we were able to achieve after optimizing the voltage waveform were 94.9%, 84.8%, and 53.5% for $\xi = 33$, 105, and 290 fJ $\cdot$ V^{-1} $\cdot$ m^{-1}, respectively. Despite our extensive effort, the switching probability could not be improved further. This can be attributed to the inherently unstable nature of VCMA switching which relies on the delicate balance between the barrier lowering effect and STT current for a carefully timed write pulse. Even though VCMA-MTJ devices have the potential for fast switching and low switching energy, the poor switching probability issue must be addressed before they can be a viable memory device. Another possible research direction is to develop VCMA material based on fundamentally different physics that will allow more robust switching. The SPICE models and run files used in this paper are available for download at mtj.umn.edu [35].

ACKNOWLEDGMENT

The authors would like to thank the SRC industry liaisons for their encouragement.

REFERENCES

[1] J.-P. Wang *et al.*, "A pathway to enable exponential scaling for the beyond-CMOS era," in *Proc. 54th Annu. Design Autom. Conf.*, Jun. 2017, Art. no. 16.

[2] S. Tehrani *et al.*, "Recent developments in magnetic tunnel junction MRAM," *IEEE Trans. Magn.*, vol. 36, no. 5, pp. 2752–2757, Sep. 2000.

[3] J.-H. Song, J. Kim, S. H. Kang, S.-S. Yoon, and S.-O. Jung, "Sensing margin trend with technology scaling in MRAM," *Int. J. Circuit Theory Appl.*, vol. 39, no. 3, pp. 313–325, 2011.

[4] S. Yuasa *et al.*, "Future prospects of MRAM technologies," in *IEDM Tech. Dig.*, Dec. 2013, pp. 3-1.1–3.1-4.

[5] D. Apalkov *et al.*, "Spin-transfer torque magnetic random access memory (STT-MRAM)," *ACM J. Emerg. Technol. Comput. Syst.*, vol. 9, no. 2, p. 13, 2013.

[6] J. H. Kim *et al.*, "Verification on the extreme scalability of STT-MRAM without loss of thermal stability below 15 nm MTJ cell," in *Symp. VLSI Technol., Dig. Tech. Papers*, Jun. 2014, pp. 1–2.

[7] E. Chen *et al.*, "Advances and future prospects of spin-transfer torque random access memory," *IEEE Trans. Magn.*, vol. 46, no. 6, pp. 1873–1878, Jun. 2010.

[8] K. Lee and S. H. Kang, "Development of embedded STT-MRAM for mobile system-on-chips," *IEEE Trans. Magn.*, vol. 47, no. 1, pp. 131–136, Jan. 2011.

[9] M. Weisheit, S. Fähler, A. Marty, Y. Souche, C. Poinsignon, and D. Givord, "Electric field-induced modification of magnetism in thin-film ferromagnets," *Science*, vol. 315, pp. 349–351, Jan. 2007.

[10] T. Maruyama *et al.*, "Large voltage-induced magnetic anisotropy change in a few atomic layers of iron," *Nature Nanotechnol.*, vol. 4, pp. 158–161, Jan. 2009.

[11] M. Endo, S. Kanai, S. Ikeda, F. Matsukura, and H. Ohno, "Electric-field effects on thickness dependent magnetic anisotropy of sputtered $MgO/Co_{40}Fe_{40}B_{20}/Ta$ structures," *Appl. Phys. Lett.*, vol. 96, no. 21, p. 212503, May 2010.

[12] W.-G. Wang, M. Li, S. Hageman, and C. L. Chien, "Electric-field-assisted switching in magnetic tunnel junctions," *Nature Mater.*, vol. 11, pp. 64–68, Nov. 2011.

[13] E. Y. Tsymbal, "Electric toggling of magnets," *Nature Mater.*, vol. 11, no. 1, pp. 12–13, Jan. 2012.

[14] N. Nishimura *et al.*, "Magnetic tunnel junction device with perpendicular magnetization films for high-density magnetic random access memory," *J. Appl. Phys.*, vol. 91, no. 8, pp. 5246–5249, 2002.

[15] T. Kishi *et al.*, "Lower-current and fast switching of a perpendicular TMR for high speed and high density spin-transfer-torque MRAM," in *IEDM Tech. Dig.*, Dec. 2008, pp. 1–4.

[16] S. Peng *et al.*, "Origin of interfacial perpendicular magnetic anisotropy in MgO/CoFe/metallic capping layer structures," *Sci. Rep.*, vol. 5, Dec. 2015, Art. no. 18173.

[17] J.-U. Thiele, L. Folks, M. F. Toney, and D. K. Weller, "Perpendicular magnetic anisotropy and magnetic domain structure in sputtered epitaxial FePt (001) $L1_0$ films," *J. Appl. Phys.*, vol. 84, no. 10, pp. 5686–5692, Nov. 1998.

[18] M. Ohtake, S. Ouchi, F. Kirino, and M. Futamoto, "Structure and magnetic properties of CoPt, CoPd, FePt, and FePd alloy thin films formed on MgO(111) substrates," *IEEE Trans. Magn.*, vol. 48, no. 11, pp. 3595–3598, Nov. 2012.

[19] S. Kanai, M. Yamanouchi, S. Ikeda, Y. Nakatani, F. Matsukura, and H. Ohno, "Electric field-induced magnetization reversal in a perpendicular-anisotropy CoFeB-MgO magnetic tunnel junction," *Appl. Phys. Lett.*, vol. 101, no. 12, p. 122403, 2012.

[20] J. Zhu *et al.*, "Voltage-induced ferromagnetic resonance in magnetic tunnel junctions," *Phys. Rev. Lett.*, vol. 108, no. 19, p. 197203, May 2012.

[21] Y. Cui, B. Khodadadi, S. Schäfer, T. Mewes, J. Lu, and S. A. Wolf, "Interfacial perpendicular magnetic anisotropy and damping parameter in ultra thin Co_2FeAl films," *Appl. Phys. Lett.*, vol. 102, no. 16, p. 162403, Apr. 2013.

[22] T. Nozaki *et al.*, "Magnetization switching assisted by high-frequency-voltage-induced ferromagnetic resonance," *Appl. Phys. Express*, vol. 7, no. 7, p. 073002, Jun. 2014.

[23] T. Nozaki *et al.*, "Large voltage-induced changes in the perpendicular magnetic anisotropy of an MgO-based tunnel junction with an ultrathin fe layer," *Phys. Rev. Appl.*, vol. 5, no. 4, p. 044006, 2016.

[24] Z. Wen, H. Sukegawa, T. Seki, T. Kubota, K. Takanashi, and S. Mitani, "Voltage control of magnetic anisotropy in epitaxial $Ru/Co_2FeAl/MgO$ heterostructures," *Sci. Rep.*, vol. 7, Mar. 2017, Art. no. 45026.

[25] P. K. Amiri *et al.*, "Electric-field-controlled magnetoelectric RAM: Progress, challenges, and scaling," *IEEE Trans. Magn.*, vol. 51, no. 11, Nov. 2015, Art. no. 3401507.

[26] C.-G. Duan *et al.*, "Surface magnetoelectric effect in ferromagnetic metal films," *Phys. Rev. Lett.*, vol. 101, p. 137201, Sep. 2008.

[27] M. K. Niranjan, C. G. Duan, S. S. Jaswal, and E. Y. Tsymbal, "Electric field effect on magnetization at the Fe/MgO(001) interface," *Appl. Phys. Lett.*, vol. 96, no. 22, p. 222504, Jun. 2010.

[28] C. Grezes *et al.*, "In-plane magnetic field effect on switching voltage and thermal stability in electric-field-controlled perpendicular magnetic tunnel junctions," *AIP Adv.*, vol. 6, no. 7, p. 075014, Jul. 2016.

[29] R. Heindl, A. Chaudhry, and S. E. Russek, "Estimation of thermal stability factor and intrinsic switching current from switching distributions in spin-transfer-torque devices with out-of-plane magnetic anisotropy," *AIP Adv.*, vol. 8, no. 1, p. 015011, Jan. 2018.

[30] K. Munira, W. H. Butler, and A. W. Ghosh, "A quasi-analytical model for energy-delay-reliability tradeoff studies during write operations in a perpendicular STT-RAM cell," *IEEE Trans. Electron Devices*, vol. 59, no. 8, pp. 2221–2226, Aug. 2012.

[31] I. Ahmed, Z. Zhao, M. G. Mankalale, S. S. Sapatnekar, J.-P. Wang, and C. H. Kim, "A comparative study between spin-transfer-torque and spin-Hall-effect switching mechanisms in PMTJ using SPICE," *IEEE J. Explor. Solid-State Computat. Devices Circuits*, vol. 3, pp. 74–82, Oct. 2017.

[32] W. Kang, Y. Ran, Y. Zhang, W. Lv, and W. Zhao, "Modeling and exploration of the voltage-controlled magnetic anisotropy effect for the next-generation low-power and high-speed MRAM applications," *IEEE Trans. Nanotechnol.*, vol. 16, no. 3, pp. 387–395, May 2017.

[33] W. H. Butler *et al.*, "Switching distributions for perpendicular spin-torque devices within the macrospin approximation," *IEEE Trans. Magn.*, vol. 48, no. 12, pp. 4684–4700, Dec. 2012.

[34] J. Kim, A. Chen, B. Behin-Aein, S. Kumar, J.-P. Wang, and C. H. Kim, "A technology-agnostic MTJ SPICE model with user-defined dimensions for STT-MRAM scalability studies," in *Proc. Custom Integr. Circuits Conf. (CICC)*, Sep. 2015, pp. 1–4.

[35] *UMN MTJ SPICE Model*. Accessed: Jun. 1, 2018. [Online]. Available: http://mtj.umn.edu

[36] S. Kanai *et al.*, "Magnetization switching in a CoFeB/MgO magnetic tunnel junction by combining spin-transfer torque and electric field-effect," *Appl. Phys. Lett.*, vol. 104, no. 21, pp. 212406.1–212406.3, May 2014.

[37] A. Sengupta, A. Jaiswal, and K. Roy, "True random number generation using voltage controlled spin-dice," in *Proc. Device Res. Conf. (DRC)*, Jun. 2016, pp. 1–2.

[38] J. G. A. Vinasco, "Voltage-controlled magnetic dynamics in nanoscale magnetic tunnel junctions," Ph.D. dissertation, Dept. Elect. Eng., Univ. California, Los Angeles, Los Angeles, CA, USA, 2014.

[39] A. Kozioł-Rachwał, T. Nozaki, K. Freindl, J. Korecki, S. Yuasa, and Y. Suzuki, "Enhancement of perpendicular magnetic anisotropy and its electric field-induced change through interface engineering in Cr/Fe/MgO," *Sci. Rep.*, vol. 7, Jul. 2017, Art. no. 5993.

[40] Z. Zhao, A. K. Smith, M. Jamali, and J.-P. Wang. (Oct. 2017). "External-field-free spin Hall switching of perpendicular magnetic nanopillar with a dipole-coupled composite structure." [Online]. Available: https://arxiv.org/abs/1603.09624

[41] S. Sharmin, A. Jaiswal, and K. Roy, "Modeling and design space exploration for bit-cells based on voltage-assisted switching of magnetic tunnel junctions," *IEEE Trans. Electron Devices*, vol. 63, no. 9, pp. 3493–3500, Sep. 2016.

[42] N. Kani, S. Rakheja, and A. Naeemi, "A probability-density function approach to capture the stochastic dynamics of the nanomagnet and impact on circuit performance," *IEEE Trans. Electron Devices*, vol. 63, no. 10, pp. 4119–4126, Oct. 2016.

[43] M. H. Jin, B. Zheng, L. Xiong, N. J. Zhou, and L. Wang, "Numerical simulations of critical dynamics in anisotropic magnetic films with the stochastic Landau-Lifshitz-Gilbert equation," *Phys. Rev. E, Stat. Phys. Plasmas Fluids Relat. Interdiscip. Top.*, vol. 98, no. 2, p. 022126, Aug. 2018.

[44] A. Vatankhahghadim, S. Huda, and A. Sheikholeslami, "A survey on circuit modeling of spin-transfer-torque magnetic tunnel junctions," *IEEE Trans. Circuits Syst. I, Reg. Papers*, vol. 61, no. 9, pp. 2634–2643, Sep. 2014.

JEEHWAN SONG received the B.E. degree in radio communications engineering from Korea University, Seoul, South Korea, in 2007, and the M.S. degree in electrical and electronic engineering from Yonsei University, Seoul, in 2009. He is currently pursuing the Ph.D. degree in electrical engineering with the University of Minnesota, Minneapolis, MN, USA.

His current research interests include mixed-signal circuit design for spin-based memories.

IBRAHIM AHMED received the B.Sc. degree in electrical and electronic engineering from the Bangladesh University of Engineering and Technology, Dhaka, Bangladesh, in 2013. He is currently pursuing the Ph.D. degree in electrical engineering with the University of Minnesota, Minneapolis, MN, USA.

His current research interests include design beyond CMOS devices and architectures and modeling of spin-based memories.

ZHENGYANG ZHAO received the B.S. degree in electrical engineering from Xi'an Jiaotong University, Xi'an, China, in 2012. He is currently pursuing the Ph.D. degree in electrical engineering with the University of Minnesota, Minneapolis, MN, USA.

His current research interests include development of novel spintronic devices for energy-efficient logic and memories.

DELIN ZHANG received the Ph.D. degree from the University of Science and Technology, Beijing, China, in 2012.

In 2012, he joined the Max Planck Institute for Chemical Physics of Solids, Dresden, Germany, as a Post-Doctoral Scientist. Since 2014, he has been a Post-Doctoral Researcher in electrical and computer engineering at the University of Minnesota, Minneapolis, MN, USA. His current research interests include exploring new perpendicular magnetic anisotropy materials and developing high-performance spintronic logic and memories.

SACHIN S. SAPATNEKAR received the Ph.D. degree from the University of Illinois at Urbana–Champaign, Champaign, IL, USA, in 1992.

He is the Henle Chair of electrical and computer engineering and the Distinguished McKnight University Professor with the University of Minnesota, Minneapolis, MN, USA.

Dr. Sapatnekar was a recipient of the NSF Career Award, seven Best Paper awards, the ICCAD Ten Year Retrospective Most Influential Paper Award, the SRC Technical Excellence award, and the SIA University Research Award.

JIAN-PING WANG received the Ph.D. degree from the Institute of Physics, Chinese Academy of Sciences, Beijing, China, in 1995, where he performed research on nanomagnetism.

He is currently the Robert Hartman Chair and a Distinguished McKnight University Professor of electrical and computer engineering, and a member of the Graduate Faculty in physics and chemical engineering, at the University of Minnesota, Minneapolis, MN, USA. He was the Director of the Center for Spintronic Materials, Interfaces, and Novel Architectures, University of Minnesota. His current research focuses on searching, fabricating, and fundamentally understanding new nanomagnetic and spintronic materials and devices.

CHRIS H. KIM received the B.S. and M.S. degrees from Seoul National University, Seoul, South Korea, and the Ph.D. degree from Purdue University, West Lafayette, IN, USA.

He is currently a Professor with the University of Minnesota, Minneapolis, MN, USA.

Dr. Kim was a recipient of the Taylor Award for Distinguished Research, SRC Technical Excellence Award, NSF CAREER Award, DAC/ISSCC Student Design Contest Awards, and IEEE Circuits and Systems Society Outstanding Young Author Award.